International Journal of Heat and Fluid Flow 29 (2008) 1593–1602

Contents lists available at ScienceDirect

International Journal of Heat and Fluid Flow

journal homepage: www.elsevier.com/locate/ijhff

Experimental Study of gas–liquid two-phase flow affected by wall surface wettability

T. Takamasa [a], T. Hazuku [a,*], T. Hibiki [b]

[a] Faculty of Marine Technology, Tokyo University of Marine Science and Technology, 2-1-6 Etchujima, Koto, Tokyo 135-8533, Japan
[b] School of Nuclear Engineering, Purdue University, 400 Central Drive, West Lafayette, IN 47907-2017, USA

ARTICLE INFO

Article history:
Received 22 August 2007
Received in revised form 9 July 2008
Accepted 10 September 2008
Available online 1 November 2008

Keywords:
Gas–liquid two-phase flow
Wall surface
Wettability
Flow regime
Flow pattern
Void fraction
Pressure drop
Drift-flux model

ABSTRACT

To evaluate the effect of wall surface wettability on the characteristics of upward gas–liquid two-phase flow in a vertical pipe, an experimental study was performed using three test pipes: an acrylic pipe, a hydrophilic pipe and a hydrophobic pipe. Basic flow characteristics such as flow patterns, pressure drop and void fraction were measured in these three pipes. In the hydrophilic pipe, a slug to churn flow transition boundary was shifted to a higher gas velocity at a given liquid velocity, whereas a churn to annular flow transition boundary was shifted to a lower gas velocity at a given liquid velocity. In the hydrophobic pipe, an inverted-churn flow regime was observed in the region where the churn flow regime was observed in the acrylic pipe, while a droplet flow regime was observed in the region where an annular flow regime was observed in the acrylic pipe. At a high gas flow rate, the mean void fraction in the hydrophobic pipe was higher than in the acrylic pipe. The effect of surface wettability on frictional pressure loss was confirmed to be insignificant under the present experimental conditions.

1. Introduction

In nuclear power plants and boilers, gas or vapor phase contained in a working two-phase flow plays an important role in determining the overall heat transfer efficiency of the system. For example, boiling heat transfer and frictional pressure loss in a system depend on the behavior and volume of the gas phase. The two-phase flow behavior is very complicated even in an adiabatic two-phase flow system. This complexity is due to the complicated interfacial forces between the two phases exerted by surface tension and fluctuations of pressure and velocity.

In recent decades, a number of researchers have pointed out the importance of the effect of wall surface wettability on gas–liquid two-phase flow characteristics. Bernardin et al. (1997) pointed out that the wall surface became superhydrophilic, or the contact angle of a water droplet became almost zero at ambient temperatures higher than 250 °C. They claimed the validity of their hypothesis with an extrapolation of their experimental results conducted in the temperature range from 20 to 170 °C. If this hypothesis is true for a heated pipe in a common boiler system or a fuel pin surface in a boiling water reactor, the heated wall surface can become superhydrophilic. On the other hand, a stable vapor film is formed on a heating wall surface when the surface temperature exceeds the Leidenfrost temperature. In such case, the heating wall surface may be close to a superhydrophobic condition. Therefore, the wall surface wettability and heat transfer associated with phase change at high temperature are expected to differ distinctly from those at room temperature. If the flow characteristics of two-phase flow are affected by a wall surface wettability, the wettability effect on the flow characteristics is one of important factors in a practical design of boiling heat transfer systems. Nonetheless, available experimental data on the effect of wall surface wettability on gas–liquid two-phase flow characteristics are limited.

Barajas and Panton (1993) pointed out that wall wettability strongly influenced the flow regime transition in a surface-tension dominated system, based on their experiment with an air–water two-phase flow in a 1.6 mm horizontal capillary tube. Iguchi and Terauchi (2001a,b) evaluated the influence of wall surface wettability on flow regime transition in vertical air–water two-phase flows in 5–15 mm diameter pipes, and proposed a bubbly-to-slug flow transition criterion for hydrophobic pipes with the contact angle higher than 100°. In addition to these studies, it should be mentioned that some studies on the effect of wettability on oil–water flows have been carried out in the field of petroleum engineering. Govier et al. (1961) obtained a flow regime map in an oil–water two-phase flow and Charles et al. (1961) developed the drift-flux correlation in a horizontal oil–water two-phase flow.

In current gas–liquid two-phase flow simulations, a viscous layer model for gas or liquid single-phase flow is usually adopted

* Corresponding author. Tel.: +81 3 5245 7727; fax: +81 3 5245 7410.
E-mail address: hazuku@kaiyodai.ac.jp (T. Hazuku).

0142-727X/$ - see front matter © 2008 Elsevier Inc. All rights reserved.
doi:10.1016/j.ijheatfluidflow.2008.09.001

Nomenclature

C	Chisholm's parameter
C_0	distribution parameter
D	pipe diameter, m
G	gravitational acceleration, m/s^2
h_d	height of sessile droplet on plate, m
h_m	height of liquid meniscus in test pipe, m
j	mixture volumetric flux, $j_g + j_f$, m/s
j_g	superficial gas velocity, m/s
j_f	superficial liquid velocity, m/s
l_d	wetting length of sessile droplet on plate, m
P	pressure, N/m^2
Re	liquid Reynolds number ($\equiv \rho_f D\langle j_f\rangle/\mu_f$)
Re_g	gas Reynolds number ($\equiv \rho_g D\langle j_g\rangle/\mu_g$)
T	total measuring time, s
T	liquid temperature, °C
t_f	time when liquid phase contacts wall surface, s
v_g	gas velocity, m/s
v_{gj}	gas drift velocity, m/s
$\overline{v_{gj}}$	mean gas drift velocity, m/s
X	Lockhart–Martinelli parameter
X	quality
Z	axial length, m

Greek symbols

A	averaged void fraction
ΔP	pressure loss, N/m^2
$\Delta\rho$	density difference between phases, kg/m^3
θ	contact angle, deg.
λ	frictional pressure coefficient
ξ	wall wettability ratio
μ_f	liquid viscosity, Ns/m^2
μ_g	gas viscosity, Ns/m^2
ρ_f	liquid density, kg/m^3
ρ_g	gas density, kg/m^3
σ	surface tension, N/m
Φ_f	two-phase multiplier

Mathematical symbols

$\langle\rangle$	area-averaged quantity
$\langle\langle\rangle\rangle$	void fraction-weighted-mean quantity

to determine the wall boundary condition. It should be noted here, however, that in a strictly sense this model may not work for two-phase flow with significant surface wettability effect on the wall or the boundary condition. Here the boundary condition of gas–liquid two-phase flow may be represented schematically using a wall contact ratio of gas and liquid phases (degree of surface wetting), ξ, defined by

$$\xi = \frac{t_{fs}}{T}, \tag{1}$$

where t_{fs} and T are, respectively, the time when liquid phase contacts the wall surface, and total measuring time. The wall wettability ratio, ξ, is unity or zero, respectively, for liquid single-phase ($x = 0$) or gas single-phase ($x = 1$) flow where x is quality (see Fig. 1). As bubble collisions with the wall and slug liquid film ruptures occur, the contact probability of the gas phase with the wall is not zero. Thus, continuous wetting wall assumption in two-phase flow may be controversial. In a similar discussion, a gas-single phase boundary condition cannot be used for mist flow as flowing liquid droplets in the gas contact the wall frequently. Therefore, it is very important to determine the boundary conditions for gas and liquid phases on the wall to perform accurate simulations of both adiabatic and boiling two-phase flow.

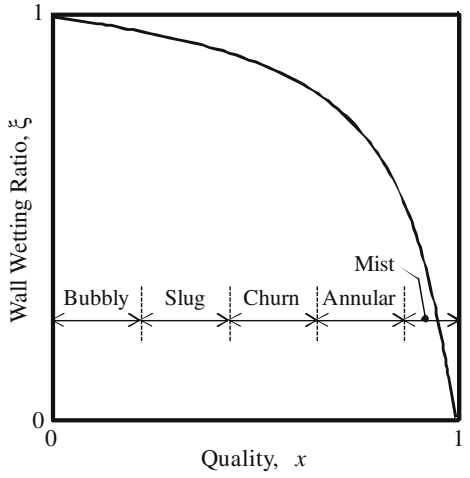

Fig. 1. Wetted wall area and boundary condition of gas–liquid two-phase flow.

For the above point of view, we examined the effect of wall surface wettability on flow characteristics in a vertical upward gas–liquid two-phase flow using three pipes with different wettability; one with an acrylic inner surface, one with a hydrophilic inner surface and one with a hydrophobic inner surface. We measured flow regime, frictional pressure loss and void fraction in these pipes and discussed the wettability effect on the flow parameters.

2. Experiment

Fig. 2 shows a schematic diagram of a vertical upward two-phase flow loop used in this study. Working fluids were air and purified tap water with an electrical conductivity controlled to be smaller than 1 μS/cm. The air was fed into the test section by a compressor. The water was pumped from a water tank through a flow meter and into the test pipe and then gravity-fed back to the water tank. Water temperature was maintained at 20 ± 2 °C by a cooler submerged in the water tank. The water temperatures in the water tank and separation tank were monitored using thermocouples with an accuracy of ±1.5 °C. Three test pipes were used; one each with a high-, a medium- and a low-wettability surface. A glass pipe coated with hydrophilic coating material (silicon dioxide-containing material, provided by Toshiba, Co.) was used as the high wettability pipe (hydrophilic pipe). An acrylic pipe was used for the medium-wettability pipe (acrylic pipe). To produce the low-wettability pipe, a water-repellent coating material (synthetic resin material, provided by NTT-AT) was applied to the inner surface of an acrylic pipe (hydrophobic pipe). The inside diameter and length of the test pipes were 20 mm and 2800 mm, including the entrance section of 1000 mm. The thickness of the coating film on the wall surface was less than 10 μm, as estimated by measuring the quantity of coating material before and after applying it. Thus, the effect of the film coating on the test pipe diameter was negligible. As an indicator of macroscopic wettability between water and wall surfaces, contact angles were estimated from Eqs. (2) and (3) based on image-processing of the meniscus image and droplet contact on the wall surface in each pipe as shown in Figs. 3 and 4. From the meniscus image, we have

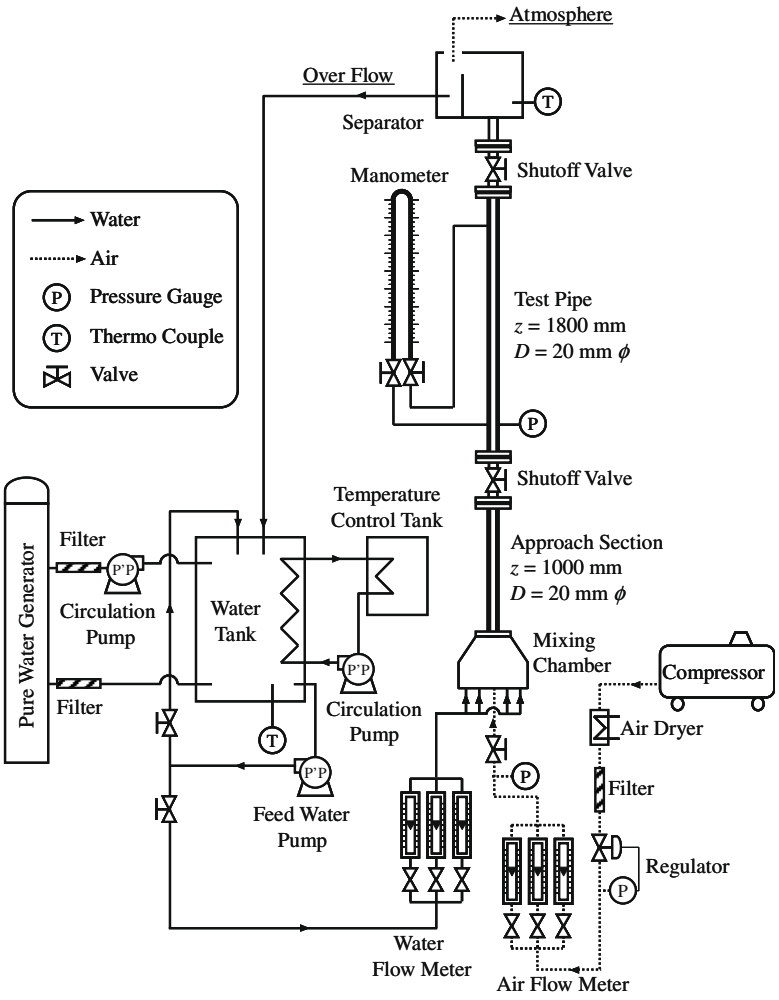

Fig. 2. Flow loop.

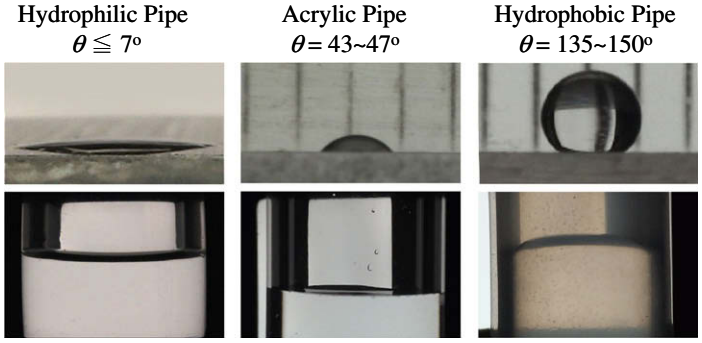

Fig. 3. Wall surface wettabilities.

$$\theta = \sin^{-1}\left[1 - \frac{\Delta\rho g h_m^2}{2\sigma}\right], \tag{2}$$

where $\Delta\rho$, g, h_m, and σ are, respectively, the density difference between phases, gravitational acceleration, height of the liquid meniscus in the test pipe, and the surface tension. From the droplet image, we have

$$\theta = 2\tan^{-1}\frac{2h_d}{l_d}, \tag{3}$$

where h_d and l_d are, respectively, the top height and wetting diameter of the water droplet. The estimated contact angles on the hydrophilic, acrylic and hydrophobic pipe surfaces were less than 7°, 45° and 146°, respectively (Fig. 3). The contact angles, surface tension and water purity were measured before and after each run to ensure the consistency in all the experiments.

The experiment was performed at a superficial gas velocity, $\langle j_g \rangle$, ranging from 0.030 to 14 m/s, and a superficial liquid velocity, $\langle j_f \rangle$, ranging from 0.050 to 2.0 m/s. The accuracy of the gas and liquid flow meters were ±5% relative to full scale conditions. Flow visualization was performed with a digital camera and a high-speed camera located at 900 mm from the test section inlet, corresponding to $z/D = 45$ where z and D are, respectively, the axial distance from the test section inlet and pipe diameter. Flow regimes in each

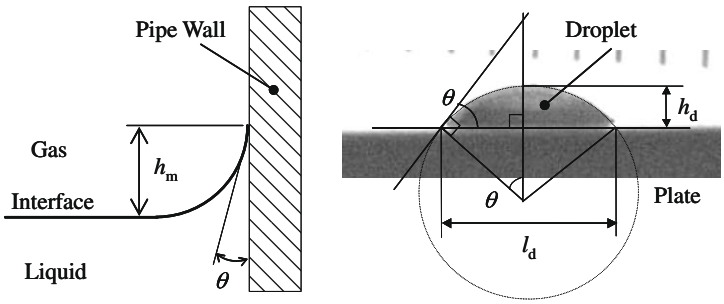

Fig. 4. Measurements of contact angle.

test pipe were determined by checking a slow replay of the motion pictures. The definitions of identified flow regimes are given in Section 3.1. When the flow regime was not clearly identified, it was defined as a flow transition regime such as bubbly to slug flow and churn to annular flow.

Differential pressure in the test pipe was measured using a glass tube manometer within an accuracy of ±12%. Two pressure extraction taps for the manometer were placed at $z = 150$ mm and 1650 mm from the inlet of the test pipe. The frictional pressure loss in two-phase flow was obtained by correcting the measured differential pressure with the water head determined from the measured void fraction. The void fraction was obtained by measuring the volumetric ratio of the gas phase remaining in the test pipe after quick shutoff of two valves installed at top and bottom of the test pipe. Since the void fractions measured in the slug and churn flow regimes varied widely, the void fraction data were obtained as an average of several test runs. In the tested conditions, the average of 3–8 test runs were enough to obtain the average void fraction within a relative deviation of ±3% from the average value. The quick shutoff valve method was also benchmarked by the differential pressure method for flow conditions where the frictional pressure drop could be neglected. Void fraction measured by two methods agreed within a relative deviation of ±5% for void fraction higher than 10%.

3. Results and discussion

3.1. Flow observation

Figs. 5–8 show typical images of flow in the hydrophilic, acrylic and hydrophobic pipes. The images in Fig. 5 were taken at the superficial gas and liquid velocities of $\langle j_g \rangle = 0.080$ m/s and $\langle j_f \rangle = 1.0$ m/s. A bubbly flow consisting of dispersed bubbles in a continuous liquid phase was observed in these test pipes. Bubbles were often observed attached to the pipe wall surface in the hydrophobic pipe. Similar trends in the bubbly flow regime with a hydrophobic pipe were reported by Iguchi and Terauchi (2001a,b).

Fig. 6 shows images taken at superficial gas and liquid velocities of $\langle j_g \rangle = 0.40$ m/s and $\langle j_f \rangle = 0.50$ m/s. A slug flow characterized by a flow alternating between a large Taylor bubble and small bubbles was observed in the hydrophilic and acrylic pipes. In the hydrophilic pipe, the film was more stable and thinner than in the acrylic pipe, as shown in the photographs. In the hydrophobic pipe, a thin liquid film that formed between the Taylor bubble and the pipe wall was destabilized and broken, resulting in a liquid rivulet flowing down the wall.

Fig. 7 shows images taken at superficial gas and liquid velocities of $\langle j_g \rangle = 3.3$ m/s and $\langle j_f \rangle = 0.30$ m/s. A churn flow with agitated liquid and gas slugs was observed in the hydrophilic and acrylic pipes. In contrast, in the hydrophobic pipe an inverted flow with reversed phase distribution in the pipe cross section was observed. In this flow, destabilized liquid jets or liquid ligaments, which were completely detached from the wall surface, flowed upward and downward in the gas core. This type of flow was previously observed in inverted-slug or inverted-churn flows in adiabatic and diabatic experiments conducted by Ishii and De Jarlais (1986, 1987), Obot and Ishii (1988), Ishii and Denten (1990).

Fig. 8 shows images taken at superficial gas and liquid velocities of $\langle j_g \rangle = 10$ m/s and $\langle j_f \rangle = 0.10$ m/s. An annular flow was observed in the acrylic and hydrophilic pipes, with a thin liquid film on the pipe wall and a continuous gas flow in the pipe core region. In contrast, no liquid film was observed on the wall of the hydrophobic pipe. The liquid phase flowed upward as droplets in a continuous gas phase. This type of flow usually occurs at relatively high-quality condition under film boiling in a heated pipe.

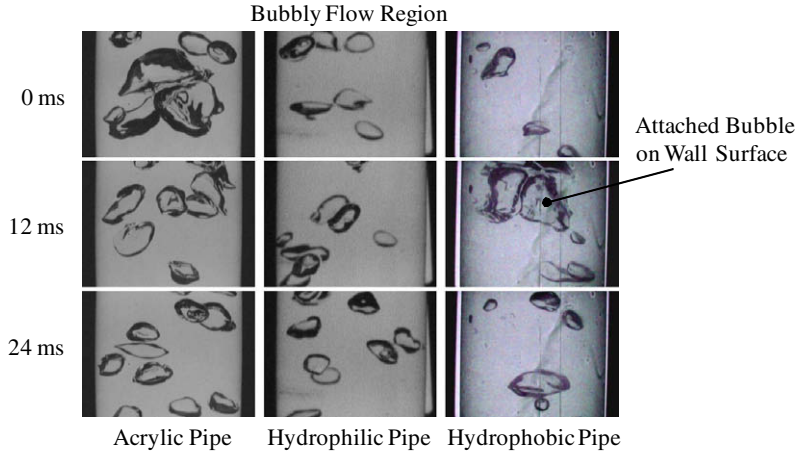

Fig. 5. Typical bubbly flow images in test pipes ($\langle j_g \rangle = 0.080$ m/s, $\langle j_f \rangle = 1.0$ m/s).

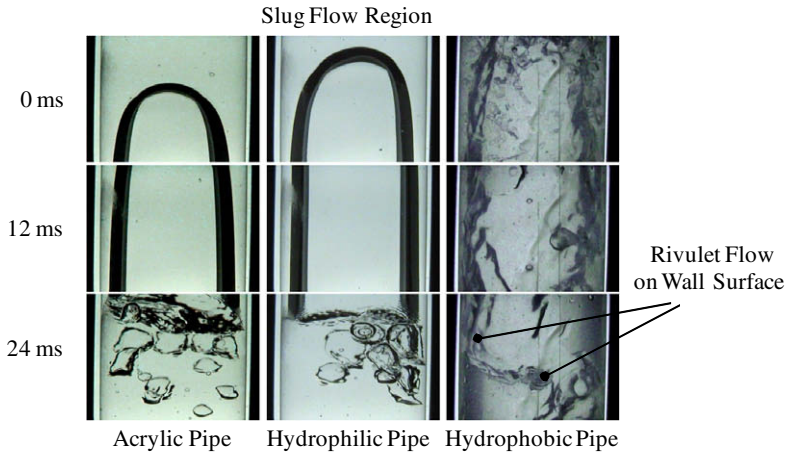

Fig. 6. Typical slug flow images in test pipes ($\langle j_g \rangle$ = 0.40 m/s, $\langle j_f \rangle$ = 0.50 m/s).

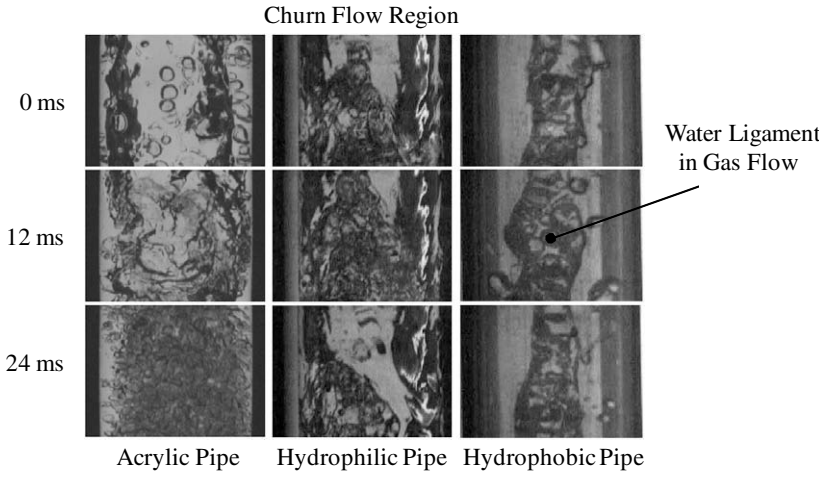

Fig. 7. Typical churn flow images in test pipes ($\langle j_g \rangle$ = 3.3 m/s, $\langle j_f \rangle$ = 0.3 m/s).

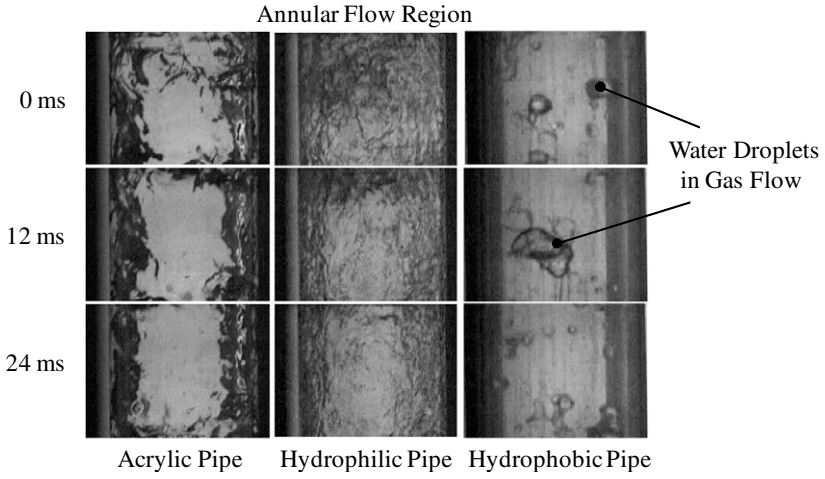

Fig. 8. Typical annular flow images in test pipes ($\langle j_g \rangle$ = 10 m/s, $\langle j_f \rangle$ = 0.10 m/s).

3.2. Flow regime

Two-phase flow regime is susceptible to inlet flow conditions and is developing along the flow direction. Hibiki and Ishii (2002b) discussed the effect of inlet bubble diameter on the flow structure in a bubbly flow regime using an interfacial area transport equation, and found that the effect of the inlet bubble size persisted even far downstream from the inlet for relatively low liquid flow rate conditions. Jeong et al. (2008) studied axial development of flow regimes in vertical upward air–water two-phase flow in an

annulus with 4.37 m length and presented an axial-location dependent flow regime map. In the experiment of Jeong et al. (2008), considerable bubble expansion due to axially reduced pressure and relatively long bubble interaction time induced some axial flow regime developments. In the present experiment, the axial location of flow visualization and inlet conditions were kept constant. Thus, comparing the flow regime maps in three pipes with different surface wettability, we can discuss the effect of the surface wettability on the flow regime.

Fig. 9a and b shows a flow regime map of an air–water two-phase flow in the acrylic pipe. The observed flow regimes are classified into four basic flow patterns: bubbly, slug, churn and annular flows. Dashed, chain, and dotted lines in Fig. 9a indicate the flow regime transition criteria based on the observations by Oshinowo and Charles (1974), Griffth and Wallis (1961), and Gould (1974), respectively. Solid and broken lines in Fig. 9b indicate the flow regime transition criteria predicted by the models of Mishima and Ishii (1984), and Taitel et al. (1980), respectively. Fig. 9c and d shows the flow regime map in the hydrophilic and hydrophobic pipes, respectively. Chain double-dashed lines in Fig. 9c and d indicate the flow regime transition boundaries observed in the current experiment using the acrylic pipe. In what follows, the dependence of the flow patterns on the surface characteristics is discussed.

3.2.1. Bubbly to slug flow transition

As shown in Fig. 9a, the bubbly to slug flow transition boundary observed in the acrylic pipe agrees with that observed by other investigators. The bubbly to slug flow transition boundaries predicted by the models of Mishima and Ishii (1984), and Taitel et al. (1980) overestimate the superficial gas velocity at the flow

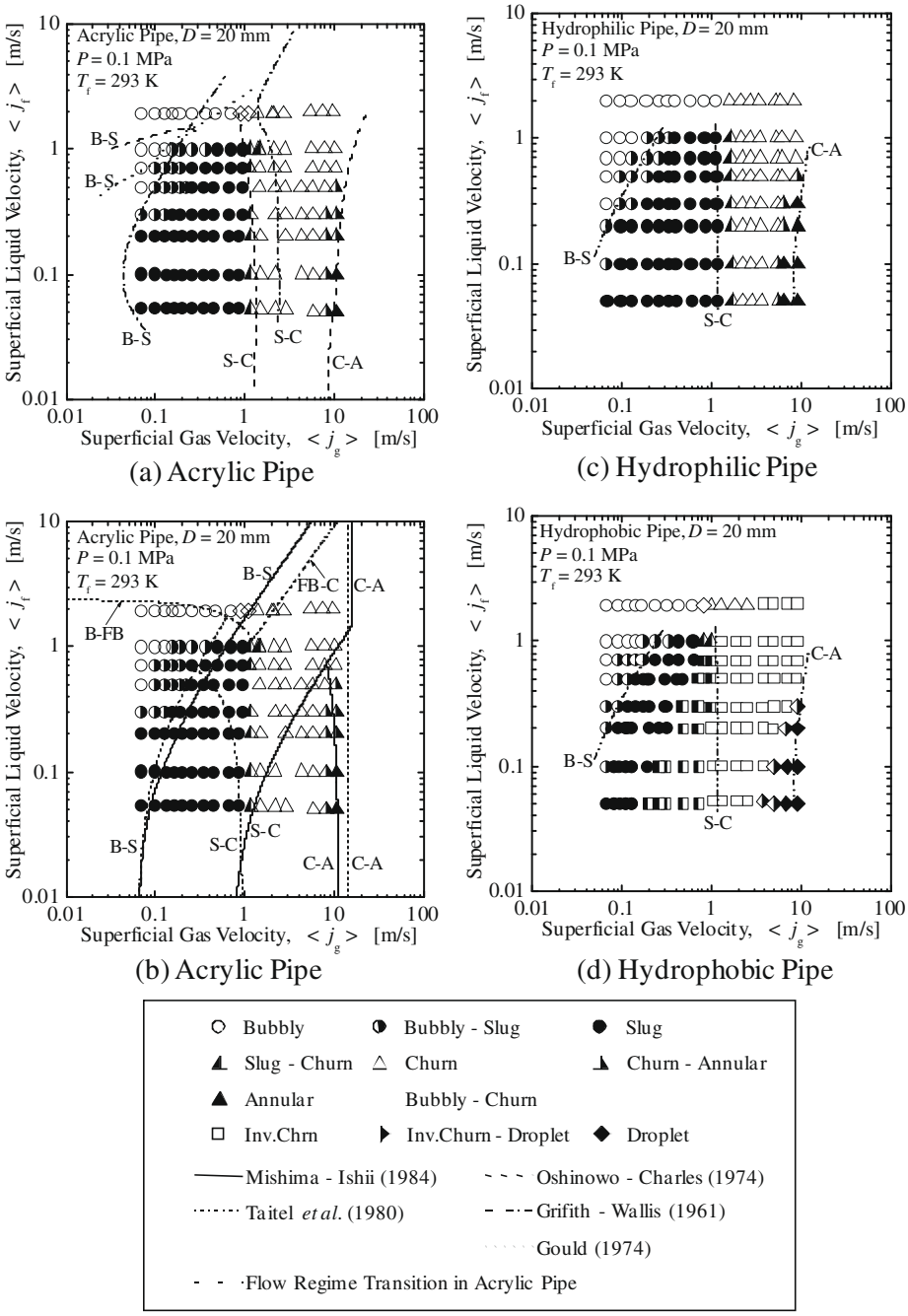

Fig. 9. Flow regime maps.

transition at a given superficial liquid velocity, which means that the bubbly to slug flow transition in the acrylic pipe occurs at a lower void fraction than in the models (Fig. 9b). However, the overall trend of the observed bubbly to slug flow transition boundary in acrylic pipe is in satisfactory agreement with the models.

As shown in the figures, for the bubbly to slug flow transition boundary there was no significant difference between the test pipes. The influence of the pipe surface characteristics on the flow pattern becomes apparent in a flow condition where gas, liquid, and solid interfaces co-exist. In the current experiment using a 20 mm diameter pipe, the ratio of such a region to the pipe cross-sectional area is relatively small, resulting in an insignificant effect of the pipe surface characteristics on the bubbly to slug flow transition boundary.

3.2.2. Slug to churn flow transition

The bubbly to slug flow transition boundary observed in the acrylic pipe agrees with that observed by other investigators (Fig. 9a). The slug to churn flow transition boundaries predicted by the models of Mishima and Ishii (1984) and Taitel et al. (1980), respectively, underestimate and overestimate the superficial gas velocity at the flow transition at a given superficial liquid velocity, which means that the observed transition boundary appears between the predictions for the two models (Fig. 9b). The tendency of the transition boundary shows a similar trend to the model of Taitel et al. (1980), which considers the axial development of the slug ascent velocity and the flow transition due to bubble coalescence. However, the overall trend of the observed slug to churn flow transition boundary in the acrylic pipe is in satisfactory agreement with the models.

As indicated in Fig. 9c, the transition boundary observed in the hydrophilic pipe occurs at a gas velocity higher than that for the transition boundary in the acrylic pipe. The hydrophilic pipe suppresses the migration of a bubble into the liquid film formed between the slug bubble and the wall, resulting in a stabilized slug bubble with a smooth surface. Such stabilized and smooth-surfaced slug bubbles suppress the chaotic interface that is often observed in the churn flow regime.

The hydrophobic pipe disrupts any liquid film, and the resulting liquid rivulet flows down the wall. This flow pattern is defined as a flow transition from slug to inverted-churn flow in the hydrophobic pipe (Fig. 9d).

3.2.3. Churn to annular flow transition

As shown in Figs. 9a and b, the churn to annular flow transition boundary observed in the acrylic pipe agrees with that observed by other investigators and predicted by the model of Mishima and Ishii (1984). A slight difference between the prediction of Taitel et al. (1980) and our observation may be due to the assumption of Taitel's model that the churn to annular flow transition occurs at the minimum gas velocity for the onset of liquid droplet formation at the interface. This criterion corresponds to the flow transition at the annular-mist flow, which occurs at a gas velocity higher than that for the onset of flow reversal.

As indicated in Fig. 9c, the transition boundary observed in the hydrophilic pipe occurs at a gas velocity lower than that for the transition boundary in the acrylic pipe, and the transition region becomes narrow. The churn flow to annular flow transition criterion is defined as the condition where the liquid slugs (that include many small bubbles) disappear and the liquid film starts rising on the wall. As mentioned above, in the hydrophilic pipe the migration of the bubbles into the liquid film is hindered and the liquid slug is more stable, resulting in the transition boundary being shifted towards a lower gas velocity.

When the flow regime transition conditions in the hydrophobic pipe match those at the churn to annular flow transition in the acrylic pipe, the flow pattern is transformed from inverted-churn flow to droplet flow. As mentioned above, the hydrophobic pipe destabilizes the liquid film in the region between slug flow and churn flow regimes, resulting in liquid rivulets. As the gas velocity increases, the liquid rivulet starts detaching from the pipe wall and flowing upward and downward in the gas. In this study, this flow regime is defined as an inverted-churn flow. Fig. 9d shows that the inverted-churn flow regime is observed at the flow condition where the churn flow regime is seen in the acrylic pipe. As the gas and liquid flow rates increase, the transition of the inverted-churn to droplet flow occurs in the hydrophobic pipe at the flow condition where the transition of churn flow to annular flow occurs in the acrylic pipe, see Fig. 9d. As shown in Fig. 8, dispersed droplets with a diameter of 2–3 mm flow in a gas core. Visual observation indicates that the droplets are formed by the breakup of the liquid jets created in the inverted-churn flow regime mainly due to interfacial instability.

3.3. Frictional pressure loss

Fig. 10 shows the measured frictional pressure coefficient of liquid single-phase flow, λ, in each test pipe. Solid and dotted lines in the figure indicate the data calculated from the conventional theoretical equations for laminar and turbulent flows, respectively. Liquid Reynolds number is defined as

$$\mathrm{Re}_\mathrm{f} = \frac{\rho_\mathrm{f}\langle j_\mathrm{f}\rangle D}{\mu_\mathrm{f}}, \tag{4}$$

where ρ_f and μ_f are the liquid density and viscosity, respectively. As shown in the figure, the frictional pressure losses in both test pipes agree with those predicted by the theoretical equations, and their dependence on the surface wall wettability is confirmed to be insignificant. This result also suggests that the effect of a change in the surface characteristics on friction pressure loss is negligible, and there is no significant change in roughness due to the hydrophilic or hydrophobic pipe coating.

The frictional pressure losses of two-phase flow are compared based on Lockhart and Martinelli's method (1949), as shown in Fig. 11. The two-phase multiplier Φ_f and the parameter X are defined as

$$\Phi_\mathrm{f} = \frac{\Delta P_T}{\Delta P_\mathrm{f}} \quad \text{and} \quad X = \frac{\Delta P_\mathrm{f}}{\Delta P_\mathrm{g}}, \tag{5}$$

where ΔP_T indicates the frictional pressure loss of two-phase flow. ΔP_f, and ΔP_g are the frictional pressure losses when either the liquid

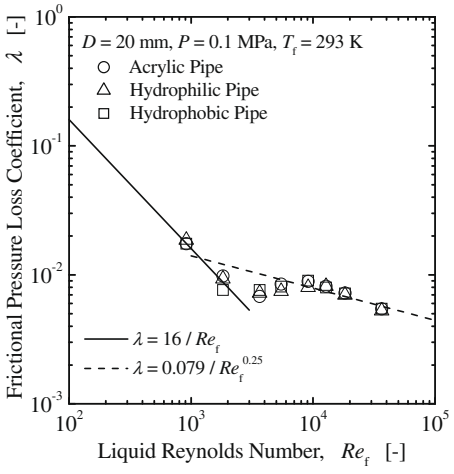

Fig. 10. Frictional pressure loss coefficient of single-phase flow.

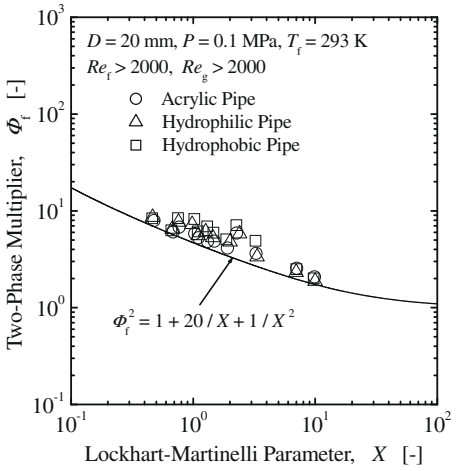

Fig. 11. Lockhart–Martinelli correlation.

or the gas component flows in the pipe as a single-phase flow, respectively. In Fig. 11, the data calculated by the following Chisholm's correction (1967) is also plotted as a reference:

$$\Phi_f^2 = 1 + \frac{C}{X} + \frac{1}{X^2}, \tag{6}$$

where C is the Chisholm's parameter being 20 for $Re_f > 2000$ and $Re_g > 2000$. Here, gas Reynolds number is defined as

$$\mathrm{Re}_g = \frac{\rho_g \langle j_g \rangle D}{\mu_g}, \tag{7}$$

where ρ_g and μ_g are the gas density and viscosity, respectively. As shown in the figure, overall trend of the measured frictional pressure loss in each test pipe agrees with that predicted by Chisholm's equation. The effect of surface wall wettability on the frictional pressure loss of two-phase flow is confirmed to be insignificant under the present experimental conditions, although the data for the hydrophobic pipe vary widely in the range of $0.5 < X < 4$, where inverted-churn flow occurs, and take a slightly higher value than in the acrylic pipe.

3.4. Average void fraction

The average void fraction obtained in the present experiment is discussed with the drift-flux model given below. The one-dimensional drift-flux model is expressed as (Zuber and Findlay, 1965)

$$\langle\langle j_g \rangle\rangle = \frac{\langle j_g \rangle}{\langle \alpha \rangle} = C_0 \langle j \rangle + \langle\langle j_{gj} \rangle\rangle, \tag{8}$$

where j_g, α, C_0, j and j_{gj} are, respectively, the gas velocity, void fraction, distribution parameter, mixture volumetric flux and drift velocity. $\langle\rangle$ and $\langle\langle\rangle\rangle$ indicate area-averaged and void fraction-weighted-mean quantities, respectively. The constitutive equations for the distribution parameter and drift velocity are given depending on the flow regime and channel (Ishii, 1977; Hibiki and Ishii, 2002a).

Bubbly flow

$$\begin{aligned} C_0 &= \left(1.2 - 0.2\sqrt{\rho_g/\rho_f}\right)\{1 - \exp(-22\langle D_{Sm}\rangle/D)\}, \\ \langle\langle j_{gj} \rangle\rangle &= \sqrt{2}(\Delta\rho g\sigma/\rho_f^2)^{1/4}(1 - \langle\alpha\rangle)^{1.75}. \end{aligned} \tag{9}$$

In Eq. (9), bubble Sauter mean diameter, D_{Sm}, can be computed by Hibiki-Ishii's correlation (2002c).

Slug flow

$$\begin{aligned} C_0 &= 1.2 - 0.2\sqrt{\rho_g/\rho_f}, \\ \langle\langle j_{gj} \rangle\rangle &= 0.35\sqrt{\Delta\rho g D/\rho_f}, \end{aligned} \tag{10}$$

Churn flow

$$\begin{aligned} C_0 &= 1.2 - 0.2\sqrt{\rho_g/\rho_f}, \\ \langle\langle j_{gj} \rangle\rangle &= \sqrt{2}(\Delta\rho g\sigma/\rho_f^2)^{1/4}. \end{aligned} \tag{11}$$

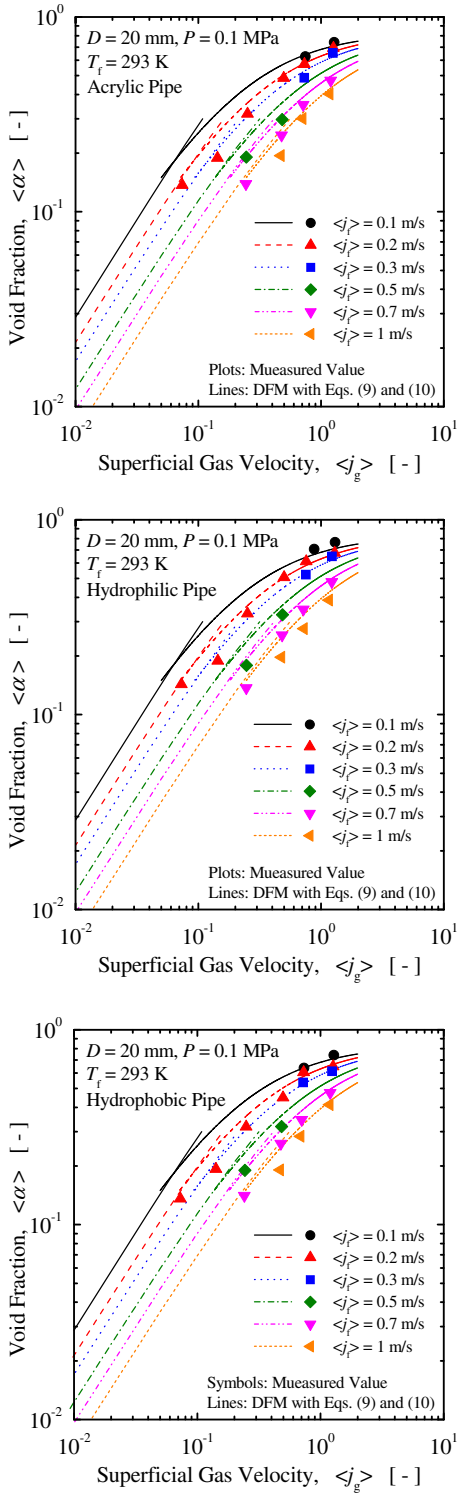

Fig. 12. Drift-flux correlation in bubbly and slug flow regimes.

Annular flow

$$\langle j_{gj}\rangle = \langle\langle j_{gj}\rangle\rangle + (C_0 - 1)\langle j\rangle = \frac{1-\langle\alpha\rangle}{\langle\alpha\rangle + \left\{\frac{1+75(1-\langle\alpha\rangle)}{\sqrt{\langle\alpha\rangle}}\frac{\rho_g}{\rho_f}\right\}^{1/2}}\left[\langle j\rangle + \sqrt{\frac{\Delta\rho g D(1-\langle\alpha\rangle)}{0.015\rho_f}}\right]. \quad (12)$$

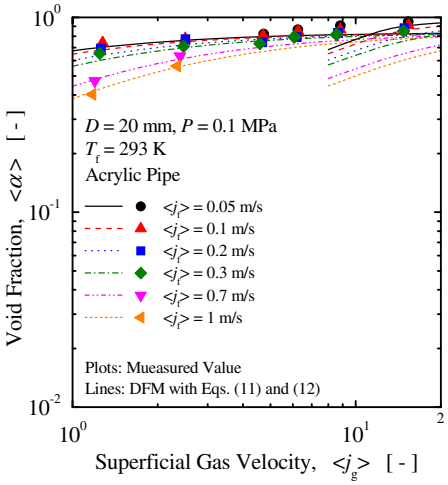

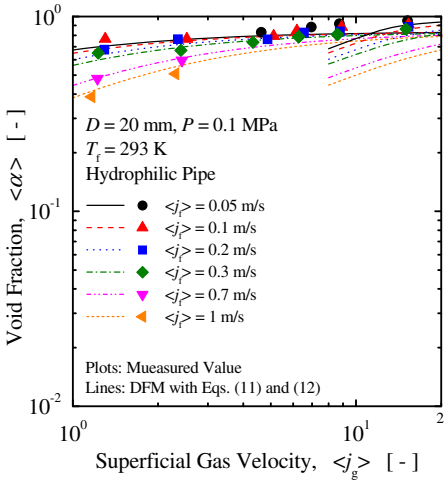

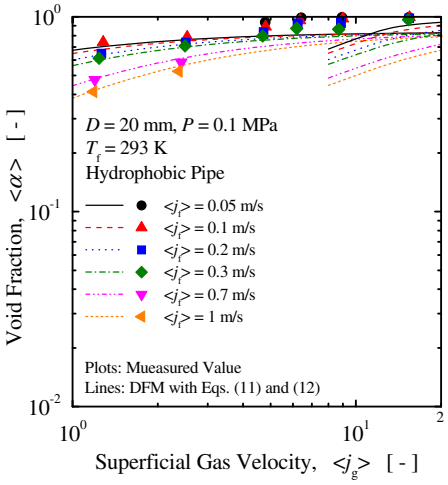

Fig. 13. Drift-flux correlation in churn and annular flow regimes.

Figs. 12 and 13 compare the drift-flux model with the data taken in bubbly and slug flow regimes and churn and annular flow regimes, respectively. Left, middle and right figures indicate the results for the acrylic pipe, hydrophilic pipe and hydrophobic pipe. As shown in the figure, the effect of surface wall wettability on the average void fraction is insignificant in bubbly flow and slug flow regions, and the measured data agree with the existing drift flux model very well. However, the void fraction data in the hydrophobic pipe show higher values than in the acrylic pipe under conditions where inverted-churn flow and droplet flow occur (Fig. 13). Most of the liquid phase in the acrylic pipe and hydrophilic pipe flows as a liquid film, subject to viscous resistance due to interaction with the pipe wall, whereas the liquid in the hydrophobic pipe flows as liquid ligaments or droplets without attaching to the pipe wall. Therefore, the relative velocity between both phases in the hydrophobic pipe should be reduced rather than that in the acrylic pipe and hydrophilic pipe. This causes the observed increase in average void fraction.

4. Conclusions

To evaluate the effect of pipe wall surface wettability on flow characteristics in a vertical upward gas–liquid two-phase flow, a visualization study was performed using three test pipes: an acrylic pipe, a hydrophilic pipe and a hydrophobic pipe. Such basic flow characteristics as flow patterns, pressure drop and void fraction were investigated in these three pipes. The results are summarized as follows:

1. In the hydrophilic pipe, the slug flow to churn flow transition boundary was shifted to a higher gas velocity at a given liquid velocity, whereas the churn flow to annular flow transition boundary was shifted to a lower gas velocity at a given liquid velocity.
2. In the hydrophobic pipe, an inverted-churn flow regime was observed in the region where the churn flow regime was observed in the acrylic pipe, while a droplet flow regime was observed in the region where an annular flow regime was observed in the acrylic pipe. At a high gas flow rate, the mean void fraction in the hydrophobic pipe was higher than in the acrylic pipe.
3. The effect of surface wettability on frictional pressure loss was confirmed to be insignificant under the present experimental conditions.

Acknowledgments

The authors wish to express special thanks to TOSHIBA Japan and NTT-AT Japan, which provided us the coating materials for the hydrophilic and hydrophobic pipes used in the experiment. The experiments were conducted with help of Messrs. N. Tamura, K. Abe and Y. Fukuhara of Tokyo University of Marine Science and Technology. Part of this work was supported by a Grant-in-Aid for Scientific Research from the Japan Society for the Promotion of Science 18760617.

References

Barajas, A.M., Panton, R.L., 1993. The effects of contact angle on two-phase flow in capillary tubes. Int. J. Multiphase Flow 19 (2), 337–346.
Bernardin, J.D., Mudawar, I., Walsh, C.B., Franses, E.I., 1997. Contact angle temperature dependence for water droplets on practical aluminum surfaces. Int. J. Heat Mass Transfer 40 (5), 1017–1033.
Chisholm, D., 1967. A theoretical basis for the Lockhart–Martinelli correlation for two-phase flow. Int. J. Heat Mass Transfer 10 (12), 1767–1778.
Charles, M.E., Govier, G.W., Hodgson, G.W., 1961. The horizontal pipe line flow of equal density oil–water mixtures. Can. J. Chem. Eng. 39, 27–36.

Govier, G.W., Sullivan, G.A., Wood, R.K., 1961. The upward vertical flow of oil–water mixtures. Can. J. Chem. Eng. 39, 67–75.
Gould, T.L., 1974. Vertical two-phase steam–water flow in geothermal wells. J. Petro. Technol. 26, 833–842.
Griffth, P., Wallis, G.B., 1961. Two-phase slug flow. Trans. ASME J. Heat Transfer 83C (3), 307–320.
Hibiki, T., Ishii, M., 2002a. Distribution parameter and drift velocity of drift-flux model in bubbly flow. Int. J. Heat Mass Transfer 45, 707–721.
Hibiki, T., Ishii, M., 2002b. Development of one-group interfacial area transport equation in bubbly flow systems. Int. J. Heat Mass Transfer 45, 2351–2372.
Hibiki, T., Ishii, M., 2002c. Interfacial area concentration of bubbly flow systems. Chem. Eng. Sci. 57, 3967–3977.
Iguchi, M., Terauchi, Y., 2001a. Boundaries among bubbly and slug flow regimes in air–water two-phase flows in vertical pipe of poor wettability. Int. J. Multiphase Flow 27 (4), 729–735.
Iguchi, M., Terauchi, Y., 2001b. Microgravity effects on the rising velocity of bubbles and slugs in vertical pipes of good and poor wettability. Int. J. Multiphase Flow 27 (12), 2189–2198.
Ishii, M., 1977. One-dimensional drift flux model and constitutive equations for relative motion between phases in various two-phase flow regimes. Argonne Natl. Lab. Report, ANL-77-47.
Ishii, M., Denten, J.P., 1990. Two-phase flow characteristic of inverted bubbly, slug and annular flow in post-critical heat flux region. Nucl. Eng. Des. 121, 349–366.
Ishii, M., De Jarlais, G., 1986. Flow regime transition and interfacial characteristics of inverted annular flow. Nucl. Eng. Des. 95, 171–184.
Ishii, M., De Jarlais, G., 1987. Flow visualization study of inverted annular flow of post dryout heat transfer region. Nucl. Eng. Des. 99, 187–199.
Jeong, J.J., Ozar, B., Dixit, A., Julia, J.E., Hibiki, T., Ishii, M., 2008. Interfacial area transport of vertical upward air–water two-phase flow in an annulus channel. Int. J. Heat Fluid Flow 29, 178–193.
Lockhart, R.W., Martinelli, R.C., 1949. Proposed correlation of data for isothermal two-phase, two-component flow in pipes. Chem. Eng. Prog. 5, 39–48.
Mishima, K., Ishii, M., 1984. Flow regime transition criteria for upward two-phase flow in vertical tubes. Int. J. Heat Mass Transfer 27 (5), 723–737.
Obot, N.T., Ishii, M., 1988. Two-phase flow regime transition criteria in post-dryout region based on flow visualization experiments. Int. J. Heat Mass Transfer 31 (12), 2559–2570.
Oshinowo, T., Charles, M.E., 1974. Vertical two-phase flow: part 2. Holdup and pressure drop. Can. J. Chem. Eng. 56, 438.
Taitel, Y., Bornea, D., Dukler, A.E., 1980. Modeling flow pattern transitions for steady upward gas–liquid flow in vertical tubes. AIChE J. 26 (3), 345–354.
Zuber, N., Findlay, J.A., 1965. Average volumetric concentration in two-phase flow systems. J. Heat Transfer 87, 453–468.